AGU PUBLICATIONS

Space Weather

REVIEW ARTICLE
10.1002/2017SW001633

Special Section:
Reprise of 2001 Space Weather Monograph

The application of heliospheric imaging to space weather operations: Lessons learned from published studies

Richard A. Harrison[1], Jackie A. Davies[1], Doug Biesecker[2], and Mark Gibbs[3]

[1]RAL Space, STFC Rutherford Appleton Laboratory, Didcot, UK, [2]NOAA Space Weather Prediction Center, Boulder, Colorado, USA, [3]UK Met Office, Exeter, UK

Key Points:
- Review of heliospheric imaging
- Assessment of the current status of the analysis of heliospheric imagery in the context of operational space weather forecasting
- Suggestions for future improvements in the exploitation of heliospheric imagery for space weather operations

Correspondence to:
R. A. Harrison,
richard.harrison@stfc.ac.uk

Citation:
Harrison, R. A., J. A. Davies, D. Biesecker, and M. Gibbs (2017), The application of heliospheric imaging to space weather operations: Lessons learned from published studies, *Space Weather*, *15*, 985–1003, doi:10.1002/2017SW001633.

Received 27 MAR 2017
Accepted 18 JUL 2017
Accepted article online 24 JUL 2017
Published online 31 AUG 2017

Abstract The field of heliospheric imaging has matured significantly over the last 10 years—corresponding, in particular, to the launch of NASA's STEREO mission and the successful operation of the heliospheric imager (HI) instruments thereon. In parallel, this decade has borne witness to a marked increase in concern over the potentially damaging effects of space weather on space and ground-based technological assets, and the corresponding potential threat to human health, such that it is now under serious consideration at governmental level in many countries worldwide. Hence, in a political climate that recognizes the pressing need for enhanced operational space weather monitoring capabilities most appropriately stationed, it is widely accepted, at the Lagrangian L1 and L5 points, it is timely to assess the value of heliospheric imaging observations in the context of space weather operations. To this end, we review a cross section of the scientific analyses that have exploited heliospheric imagery—particularly from STEREO/HI—and discuss their relevance to operational predictions of, in particular, coronal mass ejection (CME) arrival at Earth and elsewhere. We believe that the potential benefit of heliospheric images to the provision of accurate CME arrival predictions on an operational basis, although as yet not fully realized, is significant and we assert that heliospheric imagery is central to any credible space weather mission, particularly one located at a vantage point off the Sun-Earth line.

1. Introduction

Since their first successful application in the 1930s by the French astronomer Bernard Lyot, coronagraphs have been used to image the solar *K* corona—predominantly in visible light through the Thomson scatter of photospheric light from coronal electrons. Stray-light considerations place severe limitations on making such observations from the ground, necessitating in particular, a high-altitude vantage point [see, e.g. *St Cyr et al.*, 1999]. Hence, a natural progression was the installation of such instrumentation on space-based platforms. To this end, visible-light coronagraphs have been flown in space since the early 1970s (as reviewed by *Howard* [2006]), on a number of low-Earth orbiting satellites (Seventh Orbiting Solar Observatory (OSO-7) [*Koomen et al.*, 1975], Skylab [*MacQueen et al.*, 1976], Solar Maximum Mission (SMM) [*MacQueen et al.*, 1980], P78-1 [*Howard et al.*, 1985] and Spartan 201 [*Fisher and Guhathakurta*, 1994]) and, more recently, beyond Earth orbit (Solar and Heliospheric Observatory (SOHO) [*Brueckner et al.*, 1995] and Solar Terrestrial Relations Observatory (STEREO) [*Howard et al.*, 2008]). It was, in fact, the advent of spaceborne imaging of the solar corona by the coronagraph on OSO-7 that permitted the discovery of coronal mass ejections (CMEs) (*Tousey* [1973]), the phenomena now known to be associated with the most potentially destructive space weather effects (for more general information regarding the causes, potential impact—technological, societal, and economic—and mitigation of space weather effects, the reader is referred to *Eastwood et al.* [2017], *Schrijver et al.* [2015], and *Hapgood* [2017], and references therein). While the coronagraphs that have been operated from low-Earth orbit were limited, by necessity, in their operational lifetimes, those on the SOHO and STEREO spacecraft have been imaging the corona, and the CMEs therein, on a near-continuous basis for over 20 and 10 years, respectively.

For the majority of the coronagraph era, the only subsequent detection of a CME—after the first definitive observation of its eruption using a coronagraph—would be through witnessing its indirect, and convoluted, effects on planetary environments or, more directly, via its passage over one of a sparse population of space-based observatories making in situ measurements of the solar wind. CMEs have been detected in situ near Earth by, for example, the SOHO [*Domingo et al.*, 1995], Wind [*Acuna et al.*, 1995], and ACE spacecraft [*Stone et al.*, 1998] and further afield by probes at planets such as Mars and Venus and elsewhere in the heliosphere

[see, e.g., *Richardson*, 2014]. Hence, over much of the past four and a half decades, observations of the propagation and evolution of many CMEs were severely limited, covering their initial phase (within 7.5° elongation, the outer limit of the SOHO/LASCO (Large Angle Spectroscopic Coronagraph) coronagraph field of view) and supplemented only by point measurements yielded by their fortuitous passage over in situ spacecraft.

In the next section, we describe the endeavors that have been undertaken to bridge this vast observational gap, culminating in the advent of true wide-angle, visible-light heliospheric imaging. In subsequent sections, we first address the current capability of heliospheric imaging to contribute in an operational space weather context and then discuss how we believe that this capability could be improved upon.

2. Heliospheric Imaging

Recent years have seen increasing efforts to remotely sense solar wind structures, such as CMEs, beyond the confines of the corona and, instead, well into the heliosphere. One of the most abiding of these endeavors exploits the phenomenon known as interplanetary scintillation (IPS), scintillation of the signal received from a compact radio source due to the presence of density irregularities in the intervening solar wind [*Hewish et al*., 1964]. Through the monitoring of multiple sources using ground-based radio telescopes, IPS can be used to generate synoptic maps of heliospheric structure that reveal—albeit in a relatively coarse manner—background solar wind features such as stream interaction regions (SIRs), including corotating interaction regions (CIRs), and transient features such as CMEs. Such maps are now produced, for example, on a routine basis—in near real time—by the Institute for Space-Earth Environmental Research of Nagoya University, Japan, using their dedicated multistation IPS array [*Asai et al*., 1996].

Exploits in remote sensing of the heliosphere from space began somewhat later, in the 1970s, with the launch of the two Helios spacecraft. The spacecraft, in elliptical orbits around the Sun, each hosted a zodiacal light instrument [*Leinert et al*., 1981] that comprised three single-pixel, visible-light photometers, mounted 16, 31, and 90° south (Helios 1) and north (Helios 2) of the spacecraft spin plane (the ecliptic). As the spacecraft rotated, the 16° and 31° photometers scanned 32 azimuthal sectors, covering the full 360° of ecliptic longitude. Although originally intended to measure the distribution of dust in the interplanetary medium, the Helios photometers were able to trace, through Thomson scattering, the gross features of CMEs out to distances of some 0.5 AU from the Sun [e.g., *Jackson and Leinert*, 1985]. Here we must also note the pioneering work of *Sheeley et al*. [1985] who, by correlating Helios 1 observations with imagery from the Solwind coronagraph on the P78-1 satellite, demonstrated the link between CMEs in the corona and interplanetary shocks in the inner heliosphere, in particular the correlation between CME speed and shock generation.

The Helios zodiacal light photometer concept was extended into the realms of what we would now consider as true visible-light heliospheric imaging by the Solar Mass Ejection Imager (SMEI) instrument [*Eyles et al*., 2003; *T. A. Howard et al*., 2013], launched aboard the low-Earth orbiting Coriolis spacecraft in 2003. SMEI consisted of three narrow-format cameras, each with a 60° × 3° instantaneous field of view, mounted on the spacecraft such that—over the whole 102 min high-inclination orbit—the instrument provided full-sky imaging in visible light (barring an exclusion zone extending to some 18° elongation from Sun center). SMEI was designed as a proof-of-concept instrument for forecasting the arrival of CMEs and observed almost 400 CMEs before its deactivation in 2011. As well as CMEs, the SMEI images revealed other solar wind phenomena, such as SIRs/CIRs, as well as a host of other features, not all of which were expected or conducive to the instrument's objective of tracking CMEs. The latter included high-altitude aurora which, prior to SMEI, were rarely thought to be present above the 842 km orbit of Coriolis but which, it transpired, were a ubiquitous source of stray-light contamination of the SMEI images particularly during geomagnetically active conditions [e.g., *T. A. Howard et al*., 2013]; note that the severity of this contamination was, to no small degree, due to the peculiarities of the SMEI instrument design and orbital configuration. Potential contamination of the images by high-altitude aurora is not the only reason why Earth orbit is less well suited for visible-light imaging of the heliosphere—or indeed the corona—particularly, it is stressed, in an operational rather than scientific context (for more detail on the intricacies of this issue the reader is urged to refer to *DeForest and Howard* [2015]). The stray-light environment is generally more challenging in the vicinity of the Earth and its lunar companion, and the radiation environment even more so, in particular for geosynchronous/geostationary orbits; this is notwithstanding the most important issue, that being

the potentially protracted periods of complete, or partial, Earth and lunar eclipse that beset many an Earth orbit. Capitalizing on the success of the SMEI instrument, the Heliospheric Imagers (HIs) [*Eyles et al*., 2009; *Harrison et al*., 2008]—launched, in 2006, aboard NASA's twin STEREO spacecraft mission—can be considered to represent the culmination of heliospheric imaging endeavors, with the advent of truly wide-angle, visible-light imaging of the heliosphere, from a location off the Sun-Earth line. The STEREO spacecraft occupy near 1 AU heliocentric ecliptic orbits, with STEREO-A and STEREO-B, respectively, leading and trailing the Earth in its orbit (by an angle that changes by around 22.5° per year); not only is such an orbit much more benign in terms of its stray light and radiation environment than many Earth orbits, such a vantage point is, in many ways, more conducive to the imaging of Earth-directed CMEs which, when viewed side-on, tend to be brighter than their counterparts viewed head-on; this is notwithstanding the additional difficulty that can be encountered when trying to discriminate between multiple, near-contemporaneous CMEs viewed head-on (i.e., as so-called halo CMEs), the signatures of which are often superposed. The HI instrument on each STEREO spacecraft comprises two wide-angle, visible-light camera systems (HI-1 and HI-2) which, together and in nominal operations, image the heliosphere from 4 to almost 90° elongation over some 90° of position angle centered on the ecliptic plane [*Eyles et al*., 2009]. Prior to superior conjunction, HI-A (HI on STEREO-A) viewed to the east of the Sun-spacecraft line while HI-B viewed to the west. Hence—at least in the early years of the mission—both HI instruments had excellent views across the Sun-Earth line, commensurate with one of the main science objectives of the STEREO mission, which was the study of Earth-directed CMEs all the way from their launch at the Sun to impact at Earth. Since emerging from superior conjunction in 2015, the STEREO-A spacecraft has been rotated by 180° to facilitate communication with Earth, such that HI-A now views to the west of the Sun-spacecraft line (hence enabling continued viewing of the Sun-Earth line). Note that either side of superior conjunction, STEREO-A operated in a reduced telemetry mode as a result of the need to off-point the high-gain antenna (HGA) to mitigate unforeseen overheating of, in particular, the HGA feed due to the HGA's near-Sun pointing. It was during the testing of these so-called reduced operations on 1 October 2014, prior to entering superior conjunction, that contact with STEREO-B was lost due to a combination of multiple hardware anomalies; attempts to reestablish contact with STEREO-B have been partly successful and, at the time of writing, we await the imminent intensification of the recovery effort as the spacecraft approaches, albeit rather slowly, the Earth.

While it is generally accepted that recognizing solar wind structures such as CMEs (Earth bound or otherwise) in SMEI imagery can be a challenge for the less experienced user (hence, detailed analyses of SMEI data are generally the domain of users closely allied to the instrument team), the ease with which such features can be identified in STEREO/HI images has significantly enhanced the appetite for, and exploitation of, heliospheric imaging within the worldwide heliophysics community. That is, of course, not to say that the analysis of STEREO/HI images is straightforward, as the interpretation of any heliospheric imagery is fraught with potential difficulties arising, not least, from the projection effects that are inherent in viewing features out to large elongation angles via Thomson scatter (for example, the uncertainties due to the adoption of the plane-of-sky assumption, conventionally applied to coronagraph imagery, make such a naive approach untenable). The details of this will not be labored here—as they are comprehensively covered elsewhere [e.g., *Howard and DeForest*, 2012], but it is worth pointing out that, in particular, the shape and extent (and evolution thereof) assumed in the analysis of solar wind structures, such as CMEs, detected in heliospheric imaging observations can significantly modify the results of any analysis [e.g., *Davies et al*., 2012; *Rollett et al*., 2016]. However, as is elaborated upon significantly in section 4 (and with some caveats), imaging out to large elongations does enable the three-dimensional (3D) location of solar wind transients to be estimated, even based on single-spacecraft observations alone; as will also be discussed in more detail in sections 3 and 4, it is suggested that polarization measurements provide the potential to markedly improve such localization [e.g., *DeForest et al*., 2016]. So rather than being considered problematic, the SMEI and STEREO era has seen a proliferation of techniques for the analysis of heliospheric imaging observations of solar wind phenomena, some novel and others that are adaptations of methodologies previously applied to coronal imagery. This particularly applies to STEREO due to the availability of data from multiple vantage points. Many of these techniques have been developed specifically for the study of CMEs, although extensive analyses pertaining to the localization of SIRs/CIRs in heliospheric imaging data (more specifically the small-scale structures entrained within) have also been undertaken [e.g., *Rouillard et al*., 2008, 2009].

Not only has the analysis of heliospheric imagery, from the STEREO/HI instruments in particular, revealed that CMEs can be tracked out to 1 AU and beyond, even in 3D, it has also provided observational evidence that, in some cases, their kinematic properties and morphology can evolve significantly throughout their propagation, through interaction with the background solar wind, including SIRs/CIRs and fast solar wind streams, and other CMEs [e.g., *Byrne et al*., 2010; *Davis et al*., 2010; *Savani et al*., 2010; *Harrison et al*., 2012; *Lugaz et al*., 2012; *Liu et al*., 2013; *Mishra and Srivastava*, 2013; *Vršnak et al*., 2013; *Maricic et al*., 2014; *Rollett et al*., 2014; *Temmer et al*., 2014; *Wang et al*., 2014; *Zhao et al*., 2016].

3. Heliospheric Imaging in an Age of Space Weather

The coming of age of heliospheric imaging has corresponded to a period of increasing global awareness, and concern, regarding the potential risks of space weather to human technological assets and health. Response to this concern is exemplified by the following: (1) the establishment, in 2009, of ESA's Space Situational Awareness programme; (2) the release, in 2015, by the White House Office of Science and Technology Policy of a National Space Weather Strategy and a National Space Weather Action Plan for the U.S. followed by; (3) the issuing by the White House, in 2016, of Executive Order 13744: Coordinating Efforts to Prepare the Nation for Space Weather Events; and (4) the inclusion, from 2011, of space weather into the UK register of civil emergencies leading, not least, to the installation of the UK Met Office Space Weather Operations Centre, operating in parallel with the U.S. Space Weather Prediction Center.

CMEs, as noted previously, are the acknowledged drivers of the most severe space weather effects at Earth, in particular when multiple CMEs have been expelled (generally from complex active regions) and, as is increasingly becoming realized, especially when those CMEs have merged or if a CME has merged with another large-scale heliospheric structure such as a SIR/CIR [e.g., *Bothmer and Schwenn*, 1995; *Burlaga et al*., 2002; *Farrugia et al*., 2006]. Hence, their detection and the accurate prediction of their arrival at Earth (and potentially elsewhere) is of paramount importance to a credible operational space weather capability. Virtually all current operational methodologies for forecasting CME arrival at Earth (and elsewhere in the heliosphere) rely upon the characterization of their near-Sun speed and morphology in coronagraph imagery [e.g., *De Koning and Pizzo*, 2011; *Millward et al*., 2013, and references therein]. The derived CME characteristics are used to initialize solar wind propagation models that yield predictions of CME arrival time, and speed, at Earth. At the current time, the combined WSA (Wang-Sheeley-Arge) [*Arge and Pizzo*, 2000] + Enlil modeling framework provides the basis of the majority of operational CME arrival predictions [e.g., *Zheng*, 2013]. Uncertainties in characterizing CMEs—as well as the background solar wind through which they propagate (the latter is generally extrapolated from solar surface magnetic field measurements using the WSA component of the coupled model)—combined with potential breakdowns in the underlying assumptions inherent in all modeling endeavors, can lead, on occasion, to extremely poor predictions of CME arrival [e.g., *Cash et al*., 2015]. It is hence unsurprising that imaging of the heliosphere itself, and the techniques developed to analyze data therefrom, have piqued the interest of those whose concern it is to forecast space weather at Earth. In the following section, we review a cross section of the scientific analyses that have exploited heliospheric imaging observations—particularly those from STEREO/HI—noting, where pertinent, the relevance of this work to operational arrival predictions of CMEs in particular, at Earth and potentially elsewhere.

We note here that the success of heliospheric imaging in general—and in particular of STEREO/HI—has led to the inclusion of similar instrumentation on a number of scientific missions (under construction and conceptual), even in the case where the originally-proposed payload did not include such instrumentation. In particular, we note the presence of the SoloHI [*R. A. Howard et al*., 2013] and Wide-field Imager for Solar PRobe plus (WISPR) [*Vourlidas et al*., 2015] instruments on the forthcoming Solar Orbiter and Solar Probe Plus missions, respectively; WISPR is the only remote-sensing component of what is otherwise an entirely in situ payload. A number of other scientific missions, as yet unadopted, have included heliospheric imagers as either a core or indeed the sole payload component. Many of the most recent of these seek to exploit polarization, which is considered by many as the next step change in both scientific and potentially space weather usage of heliospheric imagery [*DeForest et al*., 2016]. For example, *DeForest et al*. [2010] presented a concept for a CubeSat heliospheric imaging capability in Earth orbit, called CHIME (CubeSat Heliospheric Imaging Experiment), and *Lavraud et al*. [2016] describe an L5 mission concept called INSTANT that exploits polarized heliospheric imagery.

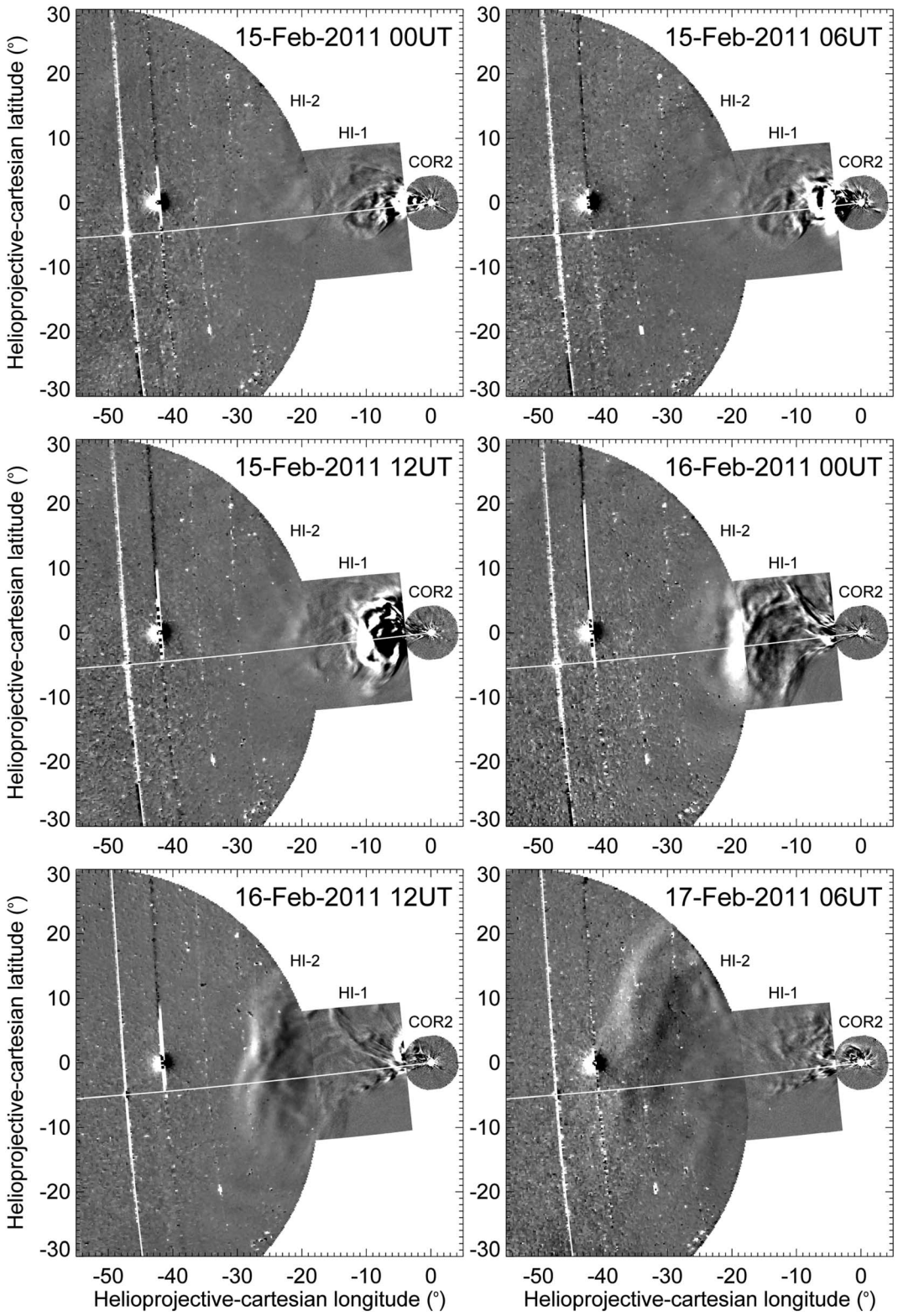

Figure 1. A sequence of six difference images from February 2011 illustrating the passage of a CME through the combined field-of-view of the STEREO-A COR2, HI-1, and HI-2 instruments. The near-horizontal white line denotes the position angle of Earth; the location of Earth corresponds to the white dot at the intersection of that line with the white near-vertical curve that corresponds to blooming along the CCD read-out direction. The signature of Venus can be seen slightly sunward, and northward, of Earth.

4. Scientific Analysis of Heliospheric Imaging Data

The advent of heliospheric imaging, in particular since the launch of the twin-spacecraft STEREO mission, has revolutionized our understanding of the evolution of CMEs as they propagate through the heliosphere. This evolution can be witnessed directly in the heliospheric images themselves, albeit with some limitations mainly due to the line-of-sight integration of the visible-light signal. Attempts to address the issues pertaining, in particular, to the localization of solar wind features (which is of specific relevance to both research and operational regimes) have spawned a plethora of techniques to aid the interpretation of heliospheric imager data, including, among many others, those by *Jackson et al*. [2006], *Kahler and Webb* [2007], *Rouillard et al*. [2008], *Sheeley et al*. [2008], *Tappin and Howard* [2009], *Byrne et al*. [2010], *Liu et al*. [2010], *Lugaz* [2010], *Lugaz et al*. [2010], *Wood et al*. [2010], *Davies et al*. [2012, 2013], *Harrison et al*. [2012], *Colaninno et al*. [2013], *Mishra and Srivastava* [2013], *Schreiner et al*. [2013], *Mishra et al*. [2014], *Möstl et al*. [2014], *Möstl and Davies* [2013], and *Rollett et al*. [2014, 2016].

In order to demonstrate the efficacy of heliospheric imaging in the detection and tracking of solar wind phenomena to Earth-like distances, Figure 1 presents a sequence of six difference images—not equally distributed in time—illustrating the passage of a CME through the combined field of view of COR2, HI-1, and HI-2 instruments on the STEREO-A spacecraft; images from the COR2 coronagraph are included in order to demonstrate the truly wide-angle nature of the HI fields of view (particularly that of HI-2). The CME, first detected by COR2 at around 2:30 UT on 15 February 2011 when the spacecraft was around 87° from the Sun-Earth line, was one of the Earth-directed CMEs considered in the study of *Colaninno et al*. [2013]. Note that the CME was preceded by two other eruptions that are visible in the first image of the series. The images are presented in helioprojective-Cartesian coordinates [*Thompson*, 2006], the Cartesian analogue of helioprojective radial coordinates (i.e., position angle and elongation); note also the that imagery has been scaled with elongation in order to compensate, to some degree, for radial expansion with increasing distance from the Sun. The near-horizontal white line denotes the position angle of Earth; Earth was at an elongation of around 48° at this time. The location of Earth itself corresponds to the intersection of that line with the white near-vertical curve corresponding to blooming of the planet's bright signal along the CCD read-out direction. Slightly sunward, and northward, of Earth can be seen the signature of Venus. It should be pointed out that this is not an optimum period for the tracking of CMEs since the Milky Way is in the HI-2 field of view.

In the 10 years since their launch, the orbital motion of the STEREO spacecraft has permitted heliospheric imaging from vantage points that cover the full range of planetary (Earth-Sun-spacecraft) angles—from 0° (when the spacecraft were close to Earth) to 180° (when they were in superior conjunction). This also includes passage through the L4 and L5 Lagrangian points, located 60° ahead of and behind the Earth, respectively. With the detection of over 1000 CMEs in the heliosphere, often stereoscopically from well-separated vantage points, the STEREO mission provides a unique facility with which to comprehensively study the evolution of CMEs during their propagation through the inner heliosphere, to 1 AU and beyond. As noted above, heliospheric imaging, in particular from the multiple vantage points afforded by STEREO, has prompted the development of a number of new techniques—as well as the modification of pre-existing methodologies, applied previously to coronal imagery—many of which are aimed at quantifying the kinematic properties of CMEs, and in particular the component of the CME propagating in the ecliptic plane. Below, we provide the reader with a flavor of the variety of approaches adopted, although we do not attempt to recount the precise details of each technique or variant thereof.

Many of the more simplistic approaches to deriving the kinematic properties of CMEs from heliospheric imager observations are based on the analysis of their time-elongation profiles, most often extracted (mainly manually, but occasionally in a more autonomous manner) along a single position angle corresponding either to the CME apex or, most commonly, to the ecliptic plane; such techniques have even been applied separately to the CME shock front, where it can be discriminated from the CME itself in the HI images [*Volpes and Bothmer*, 2015]. These techniques—which can provide information on both a CME's propagation direction within that plane (corresponding to its longitude of propagation in the case of an ecliptic time-elongation profile) and, hence, its "true" (i.e., deprojected) radial distance and speed—are underpinned by the requirement that its cross-sectional shape be prescribed; obviously, the accuracy of the derived parameters—i.e., the level of truth—depends upon the validity of the underlying assumptions. The most rudimentary approach assumes that the CME cross section can be represented as a point (the so-called

Fixed-ϕ, FP, approximation) [e.g., *Kahler and Webb*, 2007; *Rouillard et al*., 2009; *Liu et al*., 2010]. Techniques employing such an approach were soon accompanied by a suite of analogous methods in which the CME front could be characterized as a circle of finite, and potentially user-defined, angular width [e.g., *Lugaz*, 2010; *Lugaz et al*., 2010; *Davies et al*., 2012, 2013]. Such geometrical modeling techniques can be applied to the time-elongation profiles of CMEs observed from a single vantage point [e.g., *Rouillard et al*., 2009; *Lugaz*, 2010; *Davies et al*., 2012] or stereoscopically from well-separated vantage points [e.g., *Liu et al*., 2010; *Davies et al*., 2013]; the availability of observations from multiple vantage points reduces the number of assumptions required, most notably enabling time-varying—and hence more realistic—profiles of the speed of the CME front to be derived. Note also the increasing sophistication of recent analyses of this type, which have, for example, included some consideration of the "aerodynamic" drag force on the CME kinematics [e.g., *Mishra et al*., 2014; *Rollett et al*., 2016] or adopted a more realistic CME geometry [*Rollett et al*., 2016]. Some of these refinements are discussed in more detail below.

Other techniques can more naturally account for the full 3-D nature of CMEs in the heliosphere (for example, deformation, deflection, and nonradial flow), by taking into consideration visible-light observations over the entire CME front [e.g., *Jackson et al*., 2006; *Tappin and Howard*, 2009; *Byrne et al*., 2010; *Wood et al*., 2010; *Schreiner et al*., 2013]. As these techniques tend to be more time-consuming and/or computationally intensive, many have not, as yet, been as widely exploited in the analysis of CME propagation in the heliosphere as the more simplistic approaches discussed above (particularly in terms of their application to large numbers of events). Note that *Mierla et al*. [2010] review reconstruction techniques that have been applied to coronagraph imagery, some of which have subsequently been applied to heliospheric imagery; these include methods based on polarization [e.g., *De Koning and Pizzo*, 2011] of which, as yet, there are no analogous observations at heliospheric altitudes.

As for the aforementioned methods, most of these techniques also require that the geometrical form for the CME front be prescribed. Although *Schreiner et al*. [2013] assume that the CME front observed in the image can be represented by an ellipse, their method also assumes that the cross-sectional extent of the CME (i.e., its extent along the line of sight) is zero (effectively their geometry is more analogous to FP in that respect). In other cases, the CME front is considered to take the form of a 3-D elliptical shell [*Tappin and Howard*, 2009; *Byrne et al*., 2010]. One of the most commonly used full 3-D reconstruction techniques—conventionally applied to coronagraph imagery [*Thernisien et al*., 2006, 2009] but increasingly to STEREO/HI observations [e.g., *Wood et al*., 2010]—is based on the idea that the flux rope structure of a CME can be represented by the so-called Graduated Cylindrical Shell (GCS) model. Through a forward-modeling approach, the geometrical properties of the CGS flux rope formulation are refined until it best reproduces the CME topology observed in an image; this is most successfully achieved when images from multiple vantage points are available. Such fitting, when applied to a sequence of images, can provide information on a CME's true speed profile. The application of 3-D tomographic reconstruction to heliospheric visible-light imagery [e.g., *Jackson et al*., 2006] is arguably the most flexible in this respect as it requires no such prescription of the CME form. While such tomographic reconstructions has been applied extensively to SMEI data (like the Tappin-Howard model [*Tappin and Howard*, 2009]), it has not yet been applied to heliospheric imagery from STEREO.

It is also worth noting the recent successful, and systematic, application of the CACTus automatic CME detection algorithm to images from the HI-1 camera on STEREO-A [*Pant et al*., 2017]; this work was undertaken under the auspices of the HELCATS (HELiospheric Cataloguing, Analysis, and Techniques Service) project [*EU Space Research*, 2014]. Akin to the GCS model, CACTus is conventionally applied to coronagraph observations. Although applied to whole images, this does not yield 3-D information, not least because much of the potential for retrieving information in that third dimension (i.e., out of the plane of sky) from single-vantage point observations lies in the exploitation of the HI-2 imagery.

Arguably, the evolution of CMEs as they propagate through the heliosphere is most widely determined, not by observations, but through the use of the time-dependent 3-D MHD Enlil model [*Odstrcil*, 2009]. Background solar wind conditions within Enlil are generally initialized, at an inner edge of typically 21.5 solar radii, through its coupling with the WSA model, an empirical model based on the exploitation of synoptic maps of the photospheric magnetic field. The CMEs themselves are injected at the base of the numerical simulation volume through the use of a so-called cone file—into which their start time, propagation direction, angular half-width, and speed at the Enlil inner boundary are inserted—and their subsequent

evolution numerically modeled. CMEs are generally parameterized according to their appearance in coronagraph imagery, using resources such as the CAT (CME Analysis Tool) [*Millward et al*., 2013]. Obviously, the appearance of CMEs in visible-light heliospheric imagery lends itself to direct comparison with the results of such modeling; indeed, hopefully, in the future, the modeling will benefit from the direct ingestion of information on CMEs, and potentially the background solar wind, afforded by such imaging of the heliosphere. At the current time, the combined WSA-Enlil modeling framework—used in conjunction with the CAT tool—provides the basis for the majority of operational CME arrival predictions [e.g., *Zheng*, 2013; *Zhao and Dryer*, 2014].

While below we summarize some of the key results that have emerged from mainly scientific analyses of CMEs in heliospheric imaging observations, principally based on the analysis techniques described above (and concentrating, in particular, on those that provide metrics that we can more easily use to assess their space weather credentials), this discussion should not be considered as an exhaustive review of such work.

One abiding conclusion that has emerged from the analysis of heliospheric imaging observations, in particular from STEREO, is that they provide clear observationally based evidence that supports the complex evolution of the kinematics and morphology of CMEs as they propagate through the heliosphere, resulting from interactions with the background solar wind—in particular SIRs/CIRs—and, arguably more importantly, other CMEs. Such interactions, irrespective of the exact nature of the collision, have been inferred to lead to CME acceleration/deceleration, distortion and deflection [e.g., *Byrne et al*., 2010; *Davis et al*., 2010; *Savani et al*., 2010; *Harrison et al*., 2012; *Lugaz et al*., 2012; *Liu et al*., 2013; *Mishra and Srivastava*, 2013; *Vršnak et al*., 2013; *Maricic et al*., 2014; *Rollett et al*., 2014; *Temmer et al*., 2014; *Wang et al*., 2014; *Zhao et al*., 2016].

It has long been recognized, as discussed by, for example, *Millward et al*. [2013], that a single head-on view of an approaching CME (i.e., a halo CME) is not ideal, leading in particular to an ambiguity between the CME's angular width and its radial distance (corresponding to an ambiguity between its expansion speed and radial speed). In fact, resolving this ambiguity is one of the prime justifications for a synergistic approach—from both scientific and operational perspectives—that combines coronal imaging, in particular, from multiple vantage points (the most oft-quoted being a combination of L1 and L5); this has been demonstrated by combining LASCO imagery, from L1, with coronagraph imagery of CMEs from the STEREO spacecraft when the latter were appropriately located off the Sun-Earth line. However, it is also important to recognize that—in modeling the propagation of CMEs over a distance of some 200 solar radii to Earth—there is much scope for the complex propagation and evolution of CMEs to be poorly represented, through uncertainties in the initial CME and background solar wind characterization, as well as potential inadequacies in the subsequent modeling. Such a case was well demonstrated by *Cash et al*. [2015], where poorly represented conditions in the background solar wind contributed to an extremely inaccurate prediction of CME arrival; this was postulated to be due, in part, to a lack of due consideration of the level of preconditioning of interplanetary space by a preceding CME [*Temmer and Nitta*, 2015]. In an operational context, it should, of course, be noted that WSA-Enlil model runs can be used to predict CME arrival within hours of the CME eruption, therefore providing the earliest possible, potentially accurate, warning for customers (barring a sea change in our capabilities in terms of predicting CME launch).

There are a myriad of works in the published literature that demonstrate the efficacy of tracking CMEs through the heliosphere in visible light, with SMEI and, in particular, with STEREO/HI. Such observations should, in principle, be used in such a manner that they complement coronal imagery (notwithstanding the lack of a clear boundary between these two regimes, however it is defined). One example of such an analysis, by *Harrison et al*. [2012], involved the tracking of a series of four near-Earth-directed CMEs launched in quick succession on 1 August 2010. Due to an unfortunate, and extended, gap in the STEREO-B data at this time, much of the analysis concentrated on observations from STEREO-A alone (which was 78° from the Sun-Earth line at the time). Indeed, this interval is a good illustration of the utility of single-spacecraft heliospheric imagery in the analysis of Earth-directed CMEs, with an appropriately located spacecraft (in this case offset from the Sun-Earth line by an angle not far beyond the 60° of the L5 point, although located in front of rather than behind the Earth). Figure 2, which combines panels extracted from Figures 2 and 3 of *Harrison et al*. [2012], illustrates a sequence of background-subtracted HI-1 images that include elements of up to all four of the CMEs in the series as well as presenting a pair of time-elongation maps (so-called J-maps) generated in the ecliptic plane using data from both HI-1 and HI-2. The representation of heliospheric imagery in

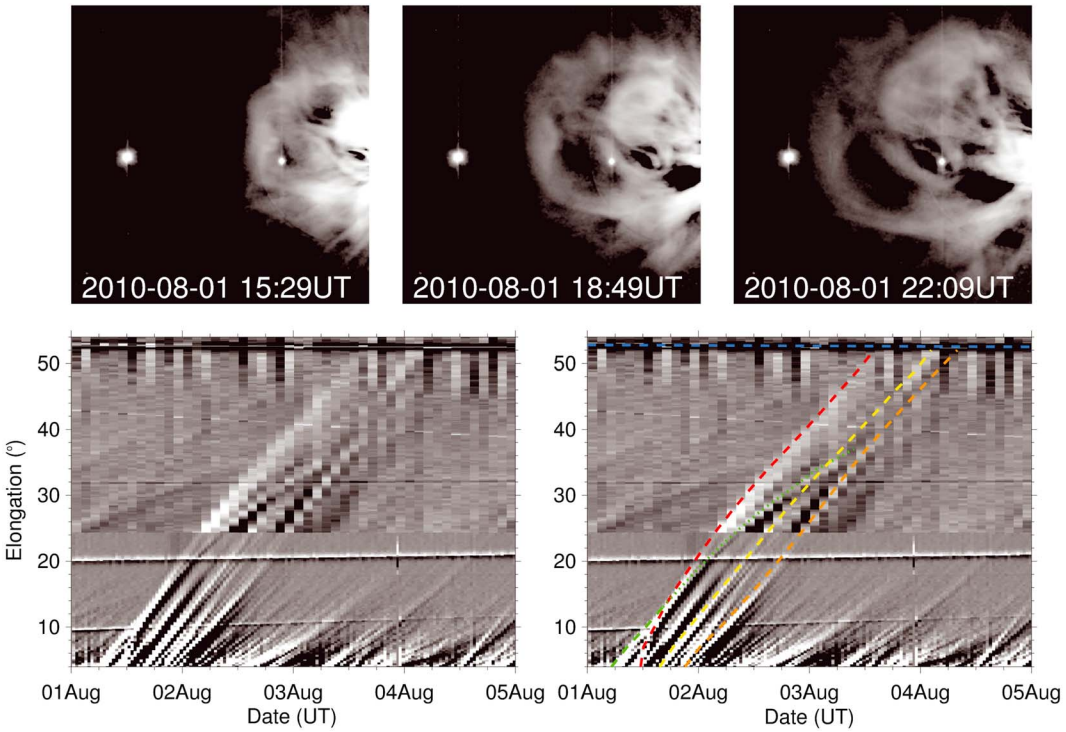

Figure 2. The series of four CMEs launched on 1 August 2010, as observed by HI on the STEREO-A spacecraft. (top) A sequence of background-subtracted images from the 20 × 20° field-of-view HI-1 camera, the boresight of which is centered in the ecliptic plane at 14° elongation (such that the Sun is 4° off the right-hand side of each image). The combined, and hence complex, visible-light signature of up to all four of the CMEs appears in the images, as do the signatures of Mercury and Venus. (bottom) Two identical time-elongation maps (J-maps), derived from ecliptic cuts through a sequence of HI-1 and HI-2 difference images. The ecliptic signatures of the four CMEs identified as having been launched on this date are highlighted by four different colored traces in the lower right-hand panel. The signatures of Mercury, Venus, and Earth are evident, as near-horizontal lines, at around 10, 20, and 53° elongation, respectively (the signature of Earth is identified explicitly using a dashed blue line) [see *Harrison et al.*, 2012].

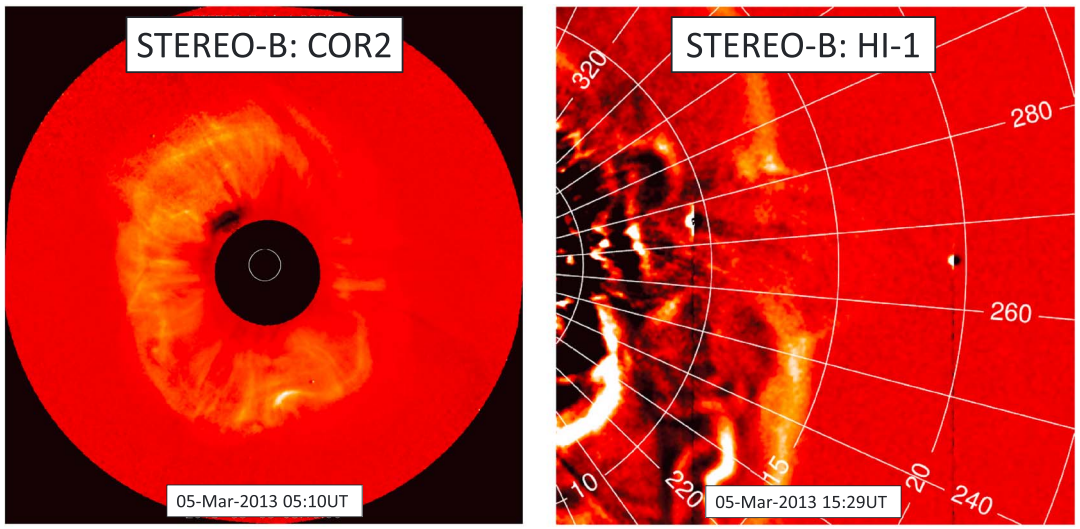

Figure 3. STEREO-B images of a halo CME launched on 5 March 2013. (left) A COR2 difference image, from 05:10 UT on that day. (right) A HI-1 difference image of the western portion of the halo event, some 10 h later.

a J-map format was pioneered by *Sheeley et al*. [2008] and *Davies et al*. [2009], extending its previous and commonplace application to coronagraph observations [*Sheeley et al*., 1999]. In such a representational format, CMEs (and other outward propagating solar wind features) are manifest as inclined traces, with a positive gradient. The ecliptic signatures of the four CMEs of this sequence are evident in the J-map which is here, as is generally done, generated using difference images; the tracks of the four CMEs are discriminated using different colored lines in the right-hand J-map, which was done with reference to the complete images. As summarized by many authors including *Davies et al*. [2012] the shape of the time-elongation profile of a solar wind transient, even when viewed from a single-spacecraft standpoint, can be analyzed (albeit based on a variety of assumptions including the prescription of an underlying geometry, as discussed above) to yield estimates of its speed and propagation direction. Such an analysis, applied to time-elongation profiles manually extracted from the HI-A ecliptic J-map, was implemented by *Harrison et al*. [2012] to demonstrate the Earth-impacting nature of three of these CMEs, the other having been subsumed by the following event within the HI-1 field of view.

The work of *Harrison et al*. [2012], and others, demonstrates several fundamental aspects that illustrate the potential value of heliospheric imaging observations to operational space weather efforts—above and beyond the fact that it can be used to track CMEs through the heliosphere, to 1 AU and beyond. CMEs observed sequentially in a coronagraph field of view can subsequently interact as they propagate through the vast portion of the inner heliosphere, invisible to coronagraphs. It is becoming increasingly understood that a CME's destructive potential, in a space weather context, can be magnified greatly when it interacts with another of its kind, or another large-scale heliospheric structure such as an interaction region (6 out of 16 of the most geoeffective events of solar cycle 23 were associated with interacting CMEs [*Farrugia et al*., 2006]). Note also, in this context, the seminal work of *Burlaga et al*. [2002] who, in studying three sets of successive halo CMEs, recognized that the complex nature of the ejecta detected in situ at L1 indicated that the CMEs had merged en route to Earth; this complexity, moreover, led the authors to conclude that the merging process was nonlinear and irreversible. The nature of the physical interaction between CMEs is uncertain, making accurate modeling even more so. This lends credence to the idea that observations within this vast, previously underexplored, region of space must (if interpreted correctly) be beneficial in an operational space weather context. The geometrical modeling that was applied by *Harrison et al*. [2012], to the ecliptic time-elongation profiles of the three CMEs that ultimately impacted Earth, not only confirmed their Earth-directed nature but also enabled the prediction of their arrival time and speed. These predictions—based on single-spacecraft data from HI-A alone, taken up to 1.8 days prior to impact—lay between 1 h 12 min and 8 h 48 min of their actual arrival time, based on their detection in situ at L1 by the Wind spacecraft. These values, which depended to some degree on the assumed extent of the CME and the exact implementation of the modeling, are in fact highly competitive when compared to the average arrival time accuracy of 7 h 30 min from WSA-Enlil quoted by *Millward et al*. [2013]. It is worth noting that the value quoted by *Millward et al*. [2013] was reliant on CME parameterization derived from CAT analysis of coronagraph imagery from two, and sometimes three, vantage points; the *Harrison et al*. [2012] study employed HI data from just one spacecraft. It should also, however, be noted that the *Millward et al*. [2013] study employed STEREO real-time data that are not of the quality of the science data products, although this is less true for the coronagraph data than for the HI data which are not particularly amenable to being heavily lossily compressed [e.g., *Davis et al*., 2009].

Not only, as noted above, does a head-on view of a CME result in ambiguity between its expansion and radial speed (notwithstanding the inherent ambiguity between front and back-sided events), such halo CMEs tend to be fainter than their counterparts viewed side-on. It should be noted here that the argument that the most potentially-destructive CMEs would likely be more dense and hence have a clearer visible-light signature, even when viewed head-on, can of course be countered by the increasing realization that (neither science nor) space weather should be limited to consideration of extreme events. The fact that CMEs are more clearly observed from the side is exemplified by the fact that only one of the four Earth-directed CMEs in the sequence of events discussed by *Harrison et al*. [2012] appears in the CDAW catalogue of LASCO-detected CMEs [https://cdaw.gsfc.nasa.gov/CME_list/]. While this also serves as additional justification for coronal imaging from multiple vantage points, the subsequent, and complex, CME evolution—including the merging of two of the CMEs prior to their arrival at Earth—could only have been revealed by complementary imaging of the heliosphere from a vantage point off the Sun-Earth line.

The work of *Harrison et al*. [2012] highlights a number of the potential benefits of heliospheric imaging, in particular from an off-Sun-Earth line viewpoint, in an operational space weather context. However, as STEREO is foremost a science mission, we must reiterate the fact that the analysis performed by the authors was based on the science data stream which, in particular for the HI instrument, is superior in terms of its quality and cadence to the low-telemetry near real-time (so-called beacon mode) data stream; the best efforts basis on which the STEREO beacon-mode data are currently retrieved is, moreover, not conducive to its continuity [*Tucker-Hood et al*., 2015]. The higher telemetry rate requirement of the STEREO science data necessitates its downlink via scheduled acquisition from the Deep Space Network; this, combined with an understandably more relaxed approach to the ground processing, means that it can be several days before the science data are generally available (obviously such an approach is not acceptable in an operational space weather scenario). However, we would advocate that the requirements for an operational heliospheric imager would need to be much more akin to the science operation of STEREO/HI rather than its beacon-mode operation [e.g., *Davis et al*., 2009; *Tucker-Hood et al*., 2015]; this would need to be borne in mind when defining an operational mission with a heliospheric imaging component to its payload.

Möstl et al. [2014] were the first authors to undertake a study of the accuracy of CME arrival predictions based on the analysis of single-spacecraft STEREO/HI time-elongation profiles, in a quasi-statistical manner. The authors studied 22 mainly Earth-directed CMEs (April 2008–July 2012), which were subsequently detected in situ, using three different model geometries—geometries that differed only in terms of the angular extent of the assumed circular CME, from a minimum of 0° (the aforementioned FP approximation) to a maximum of 180° (the so-called Harmonic Mean approach of *Lugaz* [2010]). Their predictions were based on the analysis of those HI observations that were constrained to be within 35° of Sun center (corresponding to an average lead time of 26 h). The average arrival time accuracy achieved by *Möstl et al*. [2014] was found to be 8.1 h ± 6.3 h, which improved to 6.1 ± 5.0 h when the authors applied an empirical correction based on a fit to all events. The authors found that the angular width assumed had little influence on the overall quality of the predictions; however, it should be noted that this is a partly a function of the observing geometry for Earth-directed CMEs over the interval spanning the events [*Davies et al*., 2012].

Recent years have seen an increase in the level of sophistication of techniques for the analysis of time-elongation profiles of solar wind transients. Some of these modifications, while of great benefit scientifically, are not well suited to operational implementation. For example, *Rollett et al*. [2014] used in situ measurements of CME arrival to constrain the results of their analysis. Other adaptations, however, improve the operational potential of these heliospheric imaging-based techniques, particularly in the situation where observations from only a single vantage point (or equivalently multiple closely spaced vantage points) are available; this is likely to be the case in the near future, at least. Such modifications have involved: (1) defining a more realistic CME geometry [e.g., *Rollett et al*., 2016], (2) use of external information, for example, the propagation direction from analysis of coronagraph observations, to reduce the number of free parameters that need to be derived from the HI observations alone [e.g., *Mishra et al*., 2014], and (3) inclusion of aerodynamic drag (generally based on the so-called Drag-Based Model, DBM, formulation of *Vršnak et al*. [2010]) mainly in order to extrapolate the CME speed profile beyond the realms of the HI observations [e.g., *Mishra et al*., 2014; *Rollett et al*., 2016].

While the ElEvoHI model of *Rollett et al*. [2016] potentially combines all three of these potential improvements, the authors implemented an analysis based on STEREO/HI data alone to re-examine 21 of the 22 events studied by *Möstl et al*. [2014]. ElEvoHI is underpinned by a more flexible model geometry which, through a tunable radius of curvature, can more realistically account for the "flattening" of the CME front that might be expected through interaction with preceding solar wind material [*Möstl et al*., 2015]. This, along with the other refinements such as the inclusion of drag via the DBM, yielded an improvement in the average arrival time prediction accuracy from 8.1 h of *Möstl et al*. [2014] to 6.5 h, with an even greater improvement in arrival speed. These values of arrival time accuracy are on a par with the results of the comparable single-spacecraft STEREO/HI analysis undertaken by *Mishra et al*. [2014], albeit for far fewer events, despite the fact that the latter used a propagation direction derived from stereoscopic analysis of STEREO coronagraph imagery. Note that *Mishra et al*. [2014], who also performed stereoscopic analysis of the four Earth-directed CMEs that formed the basis of their work, make the point that the performance of such stereoscopic analysis (as might be expected) surpasses that based on single-viewpoint observations alone.

In terms of a systematic comparison of CME arrival predictions based on 3-D modeling of CMEs using HI data, the work of *Colaninno et al*. [2013] is arguably the most relevant. The authors used the GCS model of *Thernisien et al*. [2009] to analyze all available visible-light imagery from both STEREO and SOHO for nine Earth-directed CMEs, observed out to a maximum of around 0.9 AU, when the STEREO spacecraft were situated between 66° and 95° of the Sun-Earth line. For these nine events, the authors extracted and fitted the deprojected time-height profile of the ecliptic portion of the CME, using a variety of different fitting methods, in order to estimate Earth arrival time and speed. Several conclusions drawn by the authors are of particular relevance to the current publication, the first of which is that when the analysis was limited to coronagraph observations, the performance was deemed disappointing (the CME arrival time was only within 12 h of the observed arrival time for three of the nine CMEs). This is surprising, considering the fact that this analysis was constrained by imagery from three vantage points. Conversely, analyses limited to observations beyond 50 solar radii (i.e., outside the coronagraph field-of-view) were found to be much more successful, with the arrival time of seven of the nine CMEs being predicted with an accuracy of within 6 h, using a simple linear fit.

The discussion above focusses, by necessity, on a relatively small selection of the most relevant works. Numerous other published (and upcoming) studies have assessed the efficacy of HI-based analysis techniques for predicting CME arrival, mainly for single or small numbers of events. Where the results of those unreferenced papers are collated within those works highlighted above, we note a broad agreement in prediction accuracy is generally found. It is also worth making the point here that when compared to 3-D CME modeling endeavors, such as tomographic reconstruction and forward modeling, the analysis techniques based on the geometrical modeling of the time-elongation profiles at a single position angle (generally the ecliptic) can be considered as fairly rudimentary; it is the ease of their implementation, and their amenability to adaptation, that has made them a popular choice for the analysis of HI data. The fact that, even when based on the use of single-spacecraft heliospheric imagery alone, these techniques are relatively competitive in terms of their CME arrival predictions (mainly at Earth), when compared with current operational methodologies, shows that there must be even greater promise when analysis of such data matures (as will be discussed in section 5 below); of course the point must again be made that the analyses are almost invariably founded on science rather than real-time data products. Note that the aforementioned HELCATS project—in which CMEs detected by the HI instruments over the entire STEREO mission to date are catalogued and their kinematic properties retrieved through a variety of modeling endeavors—is providing a test bed for the further validation of the results of such techniques [www.helcats-fp7.eu]. Obviously, the lead time of CME arrival predictions from HI observations is reduced relative to that of coronagraph observations. However, this lends itself to the idea of using HI data to continually update (and hopefully improve) a CME arrival prediction—generated by whatever means—as the CME propagates toward 1 AU; in the same vein, HI imagery could, of course, be used to update forecasts initiated using coronagraph data.

It is worth elaborating on a point made by *Colaninno et al*. [2013], who state that the CMEs in their sample tend to decelerate slowly and smoothly between 50 solar radii and 1 AU. The implication of this is, of course, that drag is the major force acting on CMEs within this regime. The authors concede—and this is an extremely important point—that this is, at least in part, due to the fact that the time range spanned by their CMEs corresponded to the rising phase of the solar cycle (cycle 24), when CMEs are energetic but not so prevalent as to result in numerous CME-CME interactions so as to confuse the measurements of individual features. This selection effect is actually determined to a large degree by the orbital configuration of STEREO; as the mission progressed beyond, say, the middle of 2011 (when the spacecraft were over 100° from the Sun-Earth line), the vantage point of the STEREO spacecraft became increasingly less well suited to the heliospheric imaging of, in particular, Earth-directed CMEs, i.e., those against which modeling techniques can be systematically validated. This is due to a number of interrelated factors, the most important being that from such a vantage point, an Earth-directed CME would tend to lie well outside the Thomson sphere, with significant impact on its visibility [*Vourlidas and Howard*, 2006; *Howard and Tappin*, 2009; *Howard and DeForest*, 2012]. The implication of *Colaninno et al*. [2013] that the increased rate of CME activity, and the associated inevitable increase in the occurrence of CME-CME interaction around solar maximum, would reduce the accuracy of their CME arrival predictions is, indeed, an obvious one. Rather than being specific to HI-based analyses, this is a generic problem, which is ironic given the

enhanced space weather potential of interacting CMEs [*Farrugia et al*., 2006]. Given the poorly understood nature of the interaction between CMEs, as recently reviewed by *Mishra et al*. [2016], it is unlikely that MHD modeling would be able to accurately predict CME arrival under such conditions. This includes the ability to account realistically for the preconditioning of the solar wind due to a preceding CME, even when the CMEs themselves do not physically interact [*Rollett et al*., 2014; *Temmer and Nitta*, 2015]. Hence, we return to the point made earlier, that particularly in an operational context, there can be no substitute for imaging the solar wind beyond the coronagraph field-of-view, even if, in its most basic form, this approach suggests use of the HI data simply as a "truth point" with which to validate MHD modeling endeavors (such midcourse monitoring and potential correction is discussed below). Such continued monitoring and updating is akin to the approach that is adopted for the passage of weather systems crossing the Atlantic, for example. Studying their development is considered to be an essential element of the forecasting activity.

The preceding discussion focuses on studies of the heliospheric propagation, and evolution, of Earth-directed CMEs based on imagery taken from a vantage point off the Sun-Earth line, from where such CMEs are best viewed. That is not to say that halo CMEs cannot be imaged in the heliosphere, much as they can at coronal altitudes. Of course, as mentioned above, the determination of CME kinematics from a single head-on view is fraught with ambiguity, ambiguity that can potentially be resolved through corresponding imagery from one or more additional vantage points. Figure 3 (left) illustrates a front-sided halo CME imaged by the COR2 coronagraph on STEREO-B, evidenced by CME expansion over the full 360° of position angle. The HI-1B image presented in Figure 3 (right) demonstrates that the same halo event can be clearly detected out beyond 15° elongation, well beyond the limit of current coronagraph fields of view. The continued tracking of halo CMEs suggests that there is value in heliospheric imaging of Earth-directed CMEs from an L1 vantage point.

5. Application of Heliospheric Imaging in an Operational Space Weather Context

It is worth reiterating, at this stage, some of the key points made above that give credence to the idea that heliospheric imaging has significant potential in an operational space weather context.

1. The signatures of CMEs can be imaged and tracked, in visible light via Thomson scatter of photospheric light, through the inner heliosphere out to 1 AU and beyond.
2. Such heliospheric imaging provides compelling observational evidence for the complex evolution of the morphology and kinematic properties of CMEs, throughout their propagation.
3. This highlights the potential contribution of heliospheric imaging, of the vast and relatively sparsely observed region between the solar corona and the Earth, in an operational space weather context.
4. Indeed, the average accuracy of CME arrival predictions from heliospheric imager-based modeling is not inconsistent with that of predictions based on more sophisticated near-Sun modeling—albeit with a shorter lead time.
5. However, noting that CME arrival predictions based on any modeling endeavor can be severely deficient—which is unacceptable in an operational scenario—we advocate a holistic approach that exploits all available observations to both monitor CMEs during their propagation, and best predict their arrival.
6. While we suggest that, for predicting space weather at Earth, the potential benefit of heliospheric imaging is maximized for a near-stationary vantage point that lies significantly (some 40° or more) off the Sun-Earth line, we also recognize the advantage of a (preferably additional) near-Earth (ideally L1) viewpoint.
7. The instrument specification—for example, field-of-view, cadence, and spatial resolution—must be carefully tailored to meet the observational requirements in order to ensure that we capitalize on the operational potential of heliospheric imaging. We must ensure that insights gleaned from a decade and a half of painstaking exploitation of SMEI and HI imagery by the science community inform this undertaking. One notable example of this is the conclusion of *DeForest and Howard* [2015] that reducing the STEREO/HI exposure time by a factor of 10 would not significantly affect the instrument noise level; this has significant implications for reducing motion blur (currently of order 1 to 3° for HI-2) [*DeForest et al*., 2011] and hence improved tracking of, for example, CME fronts.
8. We reiterate the significant, albeit as yet undemonstrated, potential of polarization measurements in improving the localization of such solar wind features as CMEs. The reader is referred, again, to the

paper of *DeForest et al*. [2016], which could be considered as a companion to the current paper in its role as the positioning paper for polarized heliospheric imaging.

6. The Future

The publications identified in the preceding sections demonstrate the potential added value, for operational space weather purposes, of the provision of heliospheric monitoring via visible-light heliospheric imaging. The question is how could the additional knowledge be most effectively utilized in a practical way as part of the forecasting process, to improve space weather forecasts? This is the next challenge, as while many space weather experts subjectively recognize the value of heliospheric images—in particular from a vantage point off the Sun-Earth line—the community will need to prove more definitively their value as an additional source of data to the forecasting process, as part of a necessary evidential chain required to fund similar observations in the future. While there are a number of potential ways in which heliospheric imagery could be exploited, those that stand out as being demonstrable, and achievable, in the imminent future are the following: (1) comparison of heliospheric imagery-based and MHD model-based J-maps; (2) use of heliospheric imagery to prune MHD model ensemble forecasts; (3) assimilation of heliospheric imagery into MHD modeling. We consider these in more detail below.

6.1. Comparison of Heliospheric Imagery-Based and MHD Model-Based J-Maps

The production of J-maps from STEREO/HI imagery, in particular, and their subsequent analysis to assess CME motion through the heliosphere, has been discussed above. The ability to simulate heliospheric images and, hence, J-maps, using output from the Enlil MHD model—however the latter is initialized—has also been demonstrated (D. Odstrčil, private communication); such simulation accounts for the theoretical aspects of Thomson scatter. In light of this capability, Figure 4 combines an ecliptic J-map derived from HI-A difference images (top right), covering the entire of March 2012, with such a synthetic J-map (bottom right). The latter is generated from the perspective of STEREO-A, for the same time period, using output from Enlil; in this case, Enlil was initialized via the standard practice of using photospheric magnetograms to define the background solar wind, through the WSA model, and using coronagraph imagery to parameterize the injected CMEs. As an example of the prevailing CME activity during this month, Figure 4 (left) presents ecliptic and meridional cuts of the modeled plasma density (top left) and radial velocity (bottom left) output by Enlil at 10 UT on 8 March, covering the arrival at Earth of a well-studied CME [e.g., *Davies et al*., 2013; *Liu et al*., 2013].

A forecaster in receipt of both real and synthetic J-maps can undertake something as straightforward as their comparison by eye. From an assessment of the relative location, and evolution thereof, of a CME in real and simulated J-maps, the forecaster could make a subjective correction to a published Enlil-derived CME arrival time prediction, bringing the arrival time forward if the heliospheric imagery indicates that the Enlil forecast is late, or, conversely, pushing the arrival time back if the Enlil forecast is early; of course this can be supplemented by comparison of real and simulated images. As new heliospheric imagery is received, and the J-maps derived therefrom updated, the CME arrival forecast could be kept under constant review and refined as appropriate. In the situation where multiple CMEs are identified, with the potential for CME-CME interaction, such data can, at the very least, provide evidence to warn of possible impending CME interaction. Forecasters would then be able to monitor the situation based on the observational evidence.

6.2. Use of Heliospheric Imagery to Prune MHD Model Ensemble Forecasts

A number of forecasting centers are currently developing Enlil ensembles of the CME parameterization envelope, the background solar wind field, or both. The advent of the ADAPT (Air Force Data Assimilative Photospheric Flux Transport) version of the WSA model [*Arge et al*., 2013] will generate 18 different, but equally valid, inner boundaries for the Enlil MHD model. Combining both the ADAPT output with a CME parameter envelope will quickly produce an ensemble run population exceeding 300 or 400 members and while many of these will cluster toward similar solutions the spread may, at times, be too large to provide useful information to guide forecasters. Figure 5 illustrates an example of ensemble output from the Enlil model —more specifically the radial speed—in which a number of runs have been undertaken based on a range of parameterizations for the injected CME (dashed lines) around a control value (shown in green). The

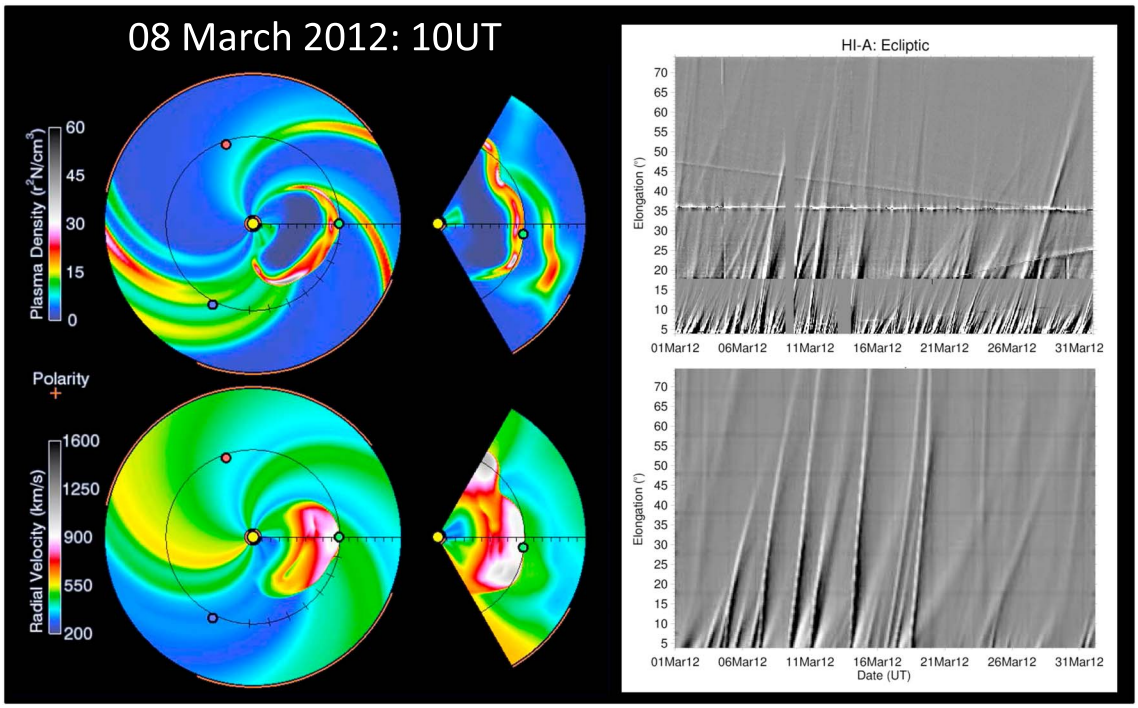

Figure 4. (top right) Ecliptic J-map derived from HI-A difference images from March 2012. (left) Ecliptic and meridional cuts of the modeled plasma density (top left) and radial velocity (bottom left) at 10 UT on 8 March 2012, output by Enlil, covering the arrival at Earth of a CME studied by, for example, *Davies et al*. [2013] and *Liu et al*. [2013]. The large yellow dot indicates the location of the Sun; smaller dots illustrate the locations of Earth (green; right), STEREO-A (red; top), and STEREO-B (blue; bottom). (bottom right) Synthetic ecliptic difference J-map from the vantage point of STEREO-A, derived from the Enlil output; such a simulated J-map can be compared to an observationally based J-map as a CME event unfolds. Note the appearance of signatures relating both to CMEs and the background solar wind in both the observed and synthetic J-maps. We thank D. Odstrčil for permission to present the Enlil results.

arrival times and speeds of the CME span ranges of some 12 h and 200 km/s, respectively. Comparison with a real J-map, as described above, could prove useful in pruning the ensemble down to a manageable number and, as new heliospheric imagery is received, the ensemble could be further pruned allowing forecasters to issue a useful CME forecast arrival range.

6.3. Assimilation of Heliospheric Imagery Into MHD Modeling

Instead of presenting information from imaging separately, in whatever form, to allow forecasters to make subjective decisions, the heliospheric imagery could potentially be assimilated into the heliospheric model itself; such assimilation is, however, challenging. One way in which this could be done is a manner analogous to what his now being done using the ground-based IPS data, which are being exploited as inner boundary values to drive 3-D MHD models including Enlil [*Jackson et al*., 2015; *Yu et al*., 2015].

Ideally, a stationary dedicated space weather spacecraft at the L5 position would provide a stable platform to allow these improvements to be most effectively realized, provided the telemetry allows near real-time transmission of a data product comparable to the current science data from STEREO/HI rather than something akin to the existing STEREO beacon-mode data.

7. Final Remarks

The maturing of the field of heliospheric imaging has corresponded to a time of increasing concern over the potentially damaging effects of space weather. In this work, we have discussed—through a review of a selected publications based mainly on the analysis of STEREO/HI observations—the potential of heliospheric imaging observations to contribute to an operational space weather mitigation scenario. Due, not least, to the evolving nature of the STEREO orbit and the sub-optimal quality of STEREO real-time (beacon) data, the operational potential of the HI instruments has not yet been fully realized. However, with the development (some of it ongoing) of a more sophisticated and holistic strategy to exploit the data therefrom, we

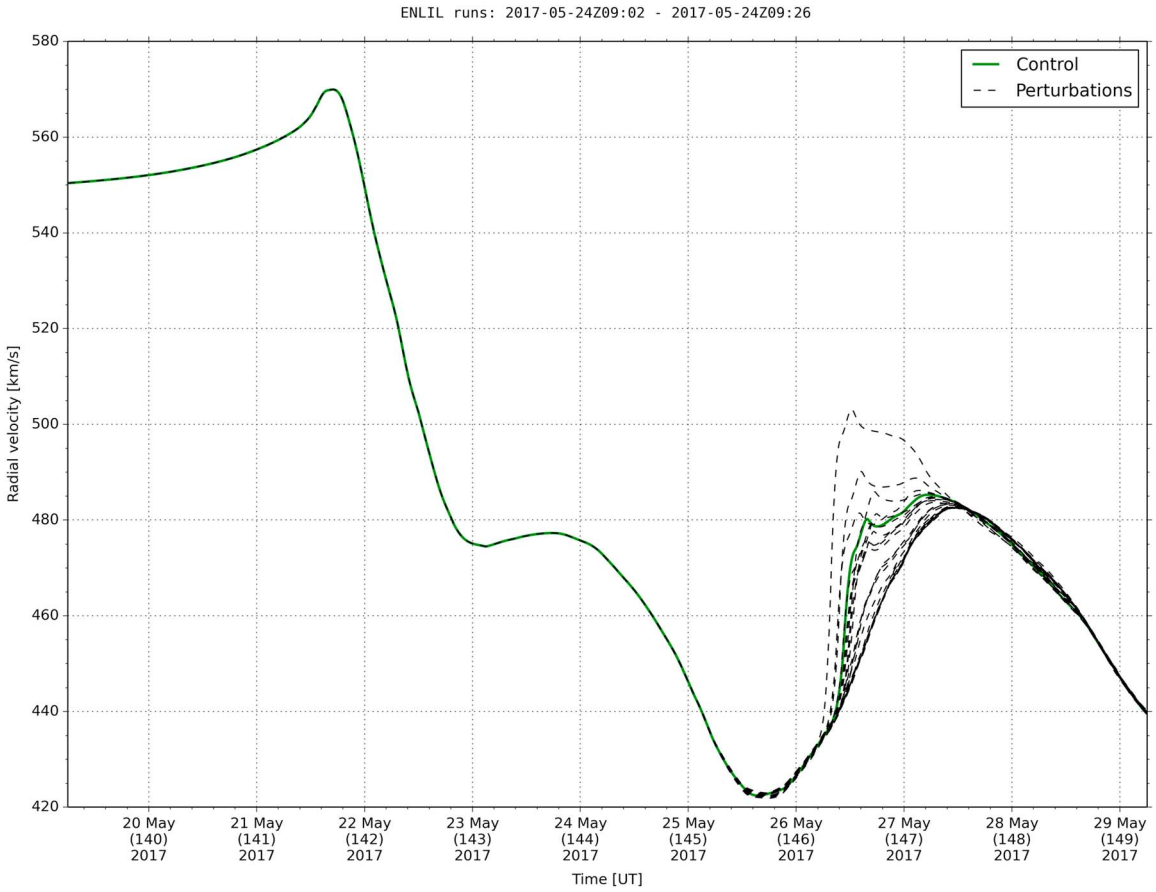

Figure 5. An example of the ensemble solar wind speed output from Enlil, for a number of runs that use a range of perturbed CME parameterizations (dashed lines) around a control (green line).

assert that heliospheric imagery is central to any credible operational space weather mission, particularly one located at a vantage point off the Sun-Earth line.

Acknowledgments

STEREO/HI was developed by an international collaboration comprising the STFC Rutherford Appleton Laboratory and the University of Birmingham (both UK), Centre Spatial de Liège (Belgium), and the Naval Research Laboratory (USA). HI is part of the multi-instrument, remote-sensing SECCHI package, developed by a consortium comprising the aforementioned institutes and also including the Lockheed Martin Solar and Astrophysics Laboratory and NASA's Goddard Space Flight Center (both USA), the Max-Planck-Institut für Sonnensystemforschung (Germany), and the Institut d'Optique Théorique et Appliquée and Institut d'Astrophysique Spatiale (both France). The STEREO/HI data are publicly available from the UK Solar System Data Centre (https://www.ukssdc.ac.uk/) and the NASA STEREO science center (https://stereo-ssc.nascom.nasa.gov/). The catalogues generated under the auspices of the HELCATS project are available from https://www.helcats-fp7.eu/.

References

Acuna, M. H., K. W. Ogilvie, D. N. Baker, S. A. Curtis, D. H. Fairfield, and W. H. Mish (1995), The Global Geospace Science Program and its investigations, *Space Sci. Rev.*, *71*, 5–21, doi:10.1007/BF00751323.

Arge, C. N., and V. J. Pizzo (2000), Improvement in the prediction of solar wind conditions using near-real time solar magnetic field updates, *J. Geophys. Res.*, *105*, 10,465–10,479, doi:10.1029/1999JA000262.

Arge, C. N., C. J. Henney, I. Gonzalez-Hernandez, W. A. Toussaint, J. Koller, and H. C. Godinez (2013), Modelling the corona and solar wind using ADAPT maps that include far-side observations, U.S. Air Force Rep. AFRL-RV-PS-TR-2014-0086.

Asai, K., Y. Ishida, M. Kojima, K. Maruyama, H. Misawa, and N. Yoshimi (1996), IPS observations at STELAB for the fruitful coming decade, *Astrophys. Space Sci.*, *243*, 247–250.

Bothmer, V., and R. Schwenn (1995), The interplanetary and solar causes of major geomagnetic storms, *J. Geomagn. Geoelectr.*, *47*, 1127–1132.

Brueckner, G. E., et al. (1995), The Large Angle Spectroscopic Coronagraph (LASCO), *Sol. Phys.*, *162*, 357–402, doi:10.1007/BF00733434.

Burlaga, L. F., S. P. Plunkett, and O. C. St Cyr (2002), Successive CMEs and complex ejecta, *J. Geophys. Res.*, *107*, 1266, doi:10.1029/2001JA000255.

Byrne, J. P., S. A. Maloney, R. T. J. McAteer, J. M. Refojo, and P. T. Gallagher (2010), Propagation of an Earth-directed coronal mass ejection in three dimensions, *Nat. Commun.*, *1*, 74, doi:10.1038/ncomms1077.

Cash, M. D., D. A. Biesecker, V. Pizzo, C. A. de Koning, G. Millward, C. N. Arge, C. J. Henney, and D. Odstrcil (2015), Ensemble modeling of the 23 July 2012 coronal mass ejection, *Space Weather*, *13*, 611–625, doi:10.1002/2015SW001232.

Colaninno, R. C., A. Vourlidas, and C. C. Wu (2013), Quantitative comparison of methods for predicting the arrival of coronal mass ejections at Earth based on multiview imaging, *J. Geophys. Res. Space Physics*, *118*, 6866–6879, doi:10.1002/2013JA019205.

Davies, J. A., R. A. Harrison, A. P. Rouillard, N. R. Sheeley, C. H. Perry, D. Bewsher, C. J. Davis, C. J. Eyles, S. Crothers, and D. S. Brown (2009), A synoptic view of solar transient evolution in the inner heliosphere using the Heliospheric Imagers on STEREO, *Geophys. Res. Lett.*, *36*, L02102, doi:10.1029/2008GL036182.

Davies, J. A., et al. (2012), A self-similar expansion model for use in solar wind transient propagation studies, *Astrophys. J.*, *750*, 23, doi:10.1088/0004-637X/750/1/23.

Davies, J. A., C. H. Perry, R. M. G. M. Trines, R. A. Harrison, N. Lugaz, C. Möstl, Y. D. Liu, and K. Steed (2013), Establishing a stereoscopic technique for determining the kinematic properties of solar wind transients based on a generalized self-similarly expanding circular geometry, *Astrophys. J.*, *777*, 167, doi:10.1088/0004-637X/777/2/167.

Davis, C. J., J. A. Davies, M. Lockwood, A. P. Rouillard, C. J. Eyles, and R. A. Harrison (2009), Stereoscopic imaging of an Earth-impacting solar coronal mass ejection: A major milestone for the STEREO mission, *Geophys. Res. Lett.*, *36*, L08102, doi:10.1029/2009GL038021.

Davis, C. J., J. Kennedy, and J. A. Davies (2010), Assessing the accuracy of CME speed and trajectory estimates from STEREO observations through a comparison of independent methods, *Sol. Phys.*, *263*, 209–222, doi:10.1007/s11207-010-9535-2.

DeForest, C., et al. (2010), The CubeSat Heliospheric Imaging Experiment (CHIME), Proc. 24th Annual AIAA/USU Conf on Small Satellites.

DeForest, C. E., and T. A. Howard (2015), Feasibility of heliospheric imaging from near Earth, *Astrophys. J.*, *804*, 126, doi:10.1088/0004-637X/804/2/126.

DeForest, C. E., T. A. Howard, and S. J. Tappin (2011), Observations of detailed structure in the solar wind at 1 AU with STEREO/HI-2, *Astrophys. J.*, *738*, 103, doi:10.1088/0004-637X/738/1/103.

DeForest, C. E., T. A. Howard, D. F. Webb, J. A. Davies, and J. A. (2016), The utility of polarized heliospheric imaging for space weather monitoring, *Space Weather*, *14*, 32–49, doi:10.1002/2015SW001286.

De Koning, C. A., and V. J. Pizzo (2011), Polarimetric localization: A new tool for calculating the CME speed and direction of propagation in near-real time, *Space Weather*, *9*, S03001, doi:10.1029/2010SW000595.

Domingo, V., B. Fleck, and A. I. Poland (1995), The SOHO mission: An overview, *Sol. Phys.*, *162*, 1–37, doi:10.1007/BF00733425.

Eastwood, J. P., E. Biffis, M. A. Hapgood, L. Green, M. M. Bisi, R. D. Bentley, R. Wicks, L.-A. McKinnell, M. Gibbs, and C. Burnett (2017), The economic impact of space weather: Where do we stand?, *Risk Anal.*, *37*, 2, doi:10.1111/risa.12765.

Eyles, C. J., G. M. Simnett, M. P. Cooke, B. V. Jackson, A. Buffington, P. P. Hick, N. R. Waltham, J. M. King, P. A. Anderson, and P. E. Holladay (2003), The Solar Mass Ejection Imager (SMEI), *Sol. Phys.*, *217*, 319–347, doi:10.1023/B:SOLA.0000006903.75671.49.

Eyles, C. J., et al. (2009), The Heliospheric Imagers onboard the STEREO mission, *Sol. Phys.*, *254*, 387–445, doi:10.1007/s11207-008-9299-0.

EU Space Research (2014), Into space, p. 113, doi:10.2769/88565.

Farrugia, C. J., H. Matsui, H. Kucharekl, V. K. Jordanova, R. B. Torbert, K. W. Ogilvie, D. B. Berichevsky, C. W. Smith, and R. Skoug (2006), Survey of intense Sun-Earth connection events (1995–2003), *Adv. Space Res.*, *38*, 498–502, doi:10.1016/j.asr.2005.05.051.

Fisher, R. R., and M. Guhathakurta (1994), Spartan 201 white light coronagraph experiment, *Space Sci. Rev.*, *70*, 267–272, doi:10.1007/BF00777878.

Hapgood, M. A. (2017), L1L5Together: Report of workshop on future missions to monitor space weather on the Sun and in the solar wind using both the L1 and L5 Lagrange points as valuable viewpoints, *Space Weather*, *15*, 654–657, doi:10.1002/2017SW001652.

Harrison, R. A., et al. (2008), First imaging of coronal mass ejections in the heliosphere viewed from outside the Sun – Earth line, *Sol. Phys.*, *247*, 171–193, doi:10.1007/s11207-007-9083-6.

Harrison, R. A., et al. (2012), An analysis of the origin and propagation of the multiple coronal mass ejections of 2010 August 1, *Astrophys. J.*, *750*, 45, doi:10.1088/0004-637X/750/1/45.

Hewish, A., P. F. Scott, and D. Wills (1964), Interplanetary scintillation of small diameter radio sources, *Nature*, *203*, 1214–1217, doi:10.1038/2031214a0.

Howard, R. A. (2006), A historical perspective on coronal mass ejections, in *Solar Eruptions and Energetic Particles*, *Geophys. Monogr. Ser.*, vol. 165, edited by N. Gopalswamy et al., pp. 7–13, AGU, Washington, D. C., doi:10.1029/GM165.

Howard, R. A., N. R. Sheeley, D. J. Michels, and M. J. Koomen (1985), Coronal mass ejections: 1979–1981, *J. Geophys. Res.*, *90*, 8173–8191, doi:10.1029/JA090iA09p08173.

Howard, R. A., et al. (2008), Sun Earth Connection Coronal and Heliospheric Investigation (SECCHI), *Space Sci. Rev.*, *136*, 67–115, doi:10.1007/s11214-008-9341-4.

Howard, R. A., et al. (2013), The Solar and Heliospheric Imager (SoloHI) instrument for the Solar Orbiter mission, Proc. SPIE 8862, Solar Physics and Space Weather Instrumentation V, doi:10.1117/12.2027657.

Howard, T. A., and C. DeForest (2012), The Thomson surface: I. Reality and myth, *Astrophys. J.*, *752*, 130, doi:10.1088/0004-637X/752/2/130.

Howard, T. A., and S. J. Tappin (2009), Interplanetary coronal mass ejections observed in the heliosphere: 3. Review of theory, *Space Sci. Rev.*, *147*, 31–54, doi:10.1007/s11214-009-9577-7.

Howard, T. A., et al. (2013), The Solar Mass Ejection Imager and its heliospheric imaging legacy, *Space Sci. Rev.*, *180*, 1–38, doi:10.1007/s11214-013-9992-7.

Jackson, B. V., and C. Leinert (1985), Helios images of solar mass ejections, *J. Geophys. Res.*, *90*, 10,759–10,764, doi:10.1029/JA090iA11p10759.

Jackson, B. V., A. Buffington, P. P. Hick, X. Wang, and D. Webb (2006), Preliminary three-dimensional analysis of the heliospheric response to the 28 October 2003 CME using SMEI white-light observations, *J. Geophys. Res.*, *111*, A04S91, doi:10.1029/2004JA010942.

Jackson, B. V., et al. (2015), The UCSD kinematic IPS solar wind boundary and its use in the Enlil 3-D MHD prediction model, *Space Weather*, *13*, 104–115, doi:10.1002/2014SW001130.

Kahler, S. W., and D. F. Webb (2007), V arc interplanetary coronal mass ejections observed with the Solar Mass Ejection Imager, *J. Geophys. Res.*, *112*, A09103, doi:10.1029/2007JA012358.

Koomen, M. J., C. R. Detwiler, G. E. Brueckner, H. W. Cooper, and R. Tousey (1975), White light coronagraph in OSO-7, *Appl. Opt.*, *14*, 743–751, doi:10.1364/AO.14.000743.

Lavraud, B., et al. (2016), A small mission concept to the Sun-Earth Lagrangian L5 point for innovative solar, heliospheric and space weather science, *J. Atmos. Sol. Terr. Phys.*, *146*, 171–185, doi:10.1016/j.jastp.2016.06.004.

Leinert, C., E. Pitz, H. Link, and N. Salm (1981), Calibration and in-flight performance of the zodiacal light experiment on HELIOS, *Space Sci. Instrum.*, *5*, 257–270.

Liu, Y., J. A. Davies, J. G. Luhmann, S. D. Bale, R. P. Lin, and A. Vourlidas (2010), Geometric triangulation of imaging observations to track coronal mass ejections continuously out to 1 AU, *Astrophys. J. Lett.*, *710*, L82–L87, doi:10.1088/2041-8205/710/1/L82.

Liu, Y. D., J. G. Luhmann, N. Lugaz, C. Mostl, J. A. Davies, S. D. Bale, and R. P. Lin (2013), On Sun-to-Earth propagation of coronal mass ejections, *Astrophys. J.*, *769*, 45, doi:10.1088/0004-637X/769/1/45.

Lugaz, N. (2010), Accuracy and limitations of fitting and stereoscopic methods to determine the direction of coronal mass ejections from heliospheric imagers observations, *Sol. Phys.*, *267*, 411–429, doi:10.1007/s11207-010-9654-9.

Lugaz, N., J. N. Hernandez-Charpak, I. I. Roussev, C. J. Davis, A. Vourlidas, and J. A. Davies (2010), Determining the azimuthal properties of coronal mass ejections from multi-spacecraft remote-sensing observations with STEREO SECCHI, *Astrophys. J.*, *715*, 493–499, doi:10.1088/0004-637X/715/1/493.

Lugaz, N., C. J. Farrugia, J. A. Davies, C. Mostl, C. J. Davis, I. I. Roussev, and M. Temmer (2012), The deflection of the two interacting coronal mass ejections of 2010 May 23–24 as revealed by combined in-situ measurements and heliospheric imaging, *Astrophys. J.*, *759*, 68, doi:10.1088/0004-637X/759/1/68.

MacQueen, R. M., J. T. Gosling, E. Hildner, R. H. Munro, A. I. Poland, and C. L. Ross (1976), Initial results from the High Altitude Observatory white light coronagraph on Skylab—A progress report, *Phil. Trans. R. Soc. Lond. A*, *281*, 405–414, doi:10.1098/rsta.1976.0038.

MacQueen, R. M., A. Csoeke-Poeckh, E. Hildner, L. L. House, R. Reynolds, A. Stanger, H. TePoel, and W. J. Wagner (1980), The high altitude observatory coronagraph/polarimeter on the solar maximum mission, *Sol. Phys.*, *65*, 91–107, doi:10.1007/BF00151386.

Maricic, D., et al. (2014), Kinematics of interacting ICMEs and related Forbush decrease: Case study, *Sol. Phys.*, *289*, 351–368, doi:10.1007/s11207-013-0314-8.

Mierla, M., et al. (2010), On the 3-D reconstruction of coronal mass ejections using coronagraph data, *Ann. Geophys.*, *28*(203–215), 2010, doi:10.5194/angeo-28-203-2010.

Millward, G., D. Biesecker, V. Pizzo, and C. A. de Koning (2013), An operational software tool for the analysis of coronagraph images: Determining CME parameters for input into the WSA-Enlil heliospheric model, *Space Weather*, *11*, 57–68, doi:10.1002/swe.20024.

Mishra, W., and N. Srivastava (2013), Estimating the arrival time of Earth-directed coronal mass ejections at in situ spacecraft using COR and HI observations from STEREO, *Astrophys. J.*, *772*, 7, doi:10.1088/0004-637X/772/1/70.

Mishra, W., N. Srivastava, and J. A. Davies (2014), A comparison of reconstruction methods for the estimation of coronal mass ejections kinematics based on SECCHI/HI observations, *Astrophys. J.*, *784*, 135, doi:10.1088/0004-637X/784/2/135.

Mishra, W., Y. Wang, and N. Srivastava (2016), On understanding the nature of collisions of coronal mass ejections observed by STEREO, *Astrophys. J.*, *831*, 99, doi:10.3847/0004-637X/831/1/99.

Möstl, C., and J. A. Davies (2013), Speeds and arrival times of solar transients approximated by self-similar expanding circular fronts, *Sol. Phys.*, *285*, 411–423, doi:10.1007/s11207-012-9978-8.

Möstl, C., et al. (2014), Connecting speeds, directions and arrival times of 22 coronal mass ejections from the Sun to 1 AU, *Astrophys. J.*, *787*, 119, doi:10.1088/0004-637X/787/2/119.

Möstl, C., et al. (2015), Strong coronal channelling and interplanetary evolution of a solar storm up to Earth and Mars, *Nat. Commun.*, *6*, 7135, doi:10.1038/ncomms8135.

Odstrcil, D. (2009), *Numerical Simulation of Interplanetary Disturbances*, *ASP Conf. Ser. 406*, edited by N. V. Pogorelov et al. "Numerical modelling of space plasma flows: ASTRONUM-2008", pp. 141–148, Astronomical Society of the Pacific, San Francisco, Calif.

Pant, V., S. Willems, L. Rodriguez, M. Mierla, D. Banerjee, and J. A. Davies (2017), Automated detection of coronal mass ejections in STEREO Heliospheric Imager data, *Astrophys. J.*, *833*, 80, doi:10.3847/1538-4357/833/1/80.

Richardson, I. G. (2014), Identification of interplanetary coronal mass ejections at Ulysses using multiple solar wind signatures, *Sol. Phys.*, *289*, 3843–3894, doi:10.1007/s11207-014-0540-8.

Rollett, T., et al. (2014), Combined multipoint remote and in situ observations of the asymmetric evolution of a fast solar coronal mass ejection, *Astrophys. J. Lett.*, *790*, L6, doi:10.1088/2041-8205/790/1/L6.

Rollett, T., C. Möstl, A. Isavnin, J. A. Davies, M. Kubicka, U. V. Amerstorfer, and R. A. Harrison (2016), ElEvoHI: A novel CME prediction tool for heliospheric imaging combining an elliptical front with drag-based model fitting, *Astrophys. J.*, *824*, 131, doi:10.3847/0004-637X/824/2/131.

Rouillard, A. P., et al. (2008), First imaging of corotating interaction regions using the STEREO spacecraft, *Geophys. Res. Lett.*, *35*, L10110, doi:10.1029/2008GL033767.

Rouillard, A. P., et al. (2009), A solar storm observed from the Sun to Venus using STEREO, Venus Express and MESSENGER spacecraft, *J. Geophys. Res.*, *114*, A07106, doi:10.1029/2008JA014034.

Savani, N., M. Owens, A. P. Rouillard, R. Forsyth, and J. A. Davies (2010), Observational evidence of a CME distortion directly attributable to a structured solar wind, *Astrophys. J. Lett.*, *714*, L128–L132, doi:10.1088/2041-8205/714/1/L128.

Schreiner, S., C. Cattell, K. Kersten, and A. Hupach (2013), Using an ellipsoid model to track and predict the evolution and propagation of coronal mass ejections, *Sol. Phys.*, *288*, 291–309, doi:10.1007/s11207-012-9936-5.

Schrijver, C. J., et al. (2015), Understanding space weather to shield society: A global roadmap for 2015–2025 commissioned by COSPAR and ILWS, *Adv. Space Res. 55*, 2745–2807, doi:10.1016/j.asr.2015.03.023.

Sheeley, N. R., Jr., R. A. Howard, M. J. Koomen, D. J. Michels, R. Schwenn, K. H. Mühlhäuser, and H. Rosenbauer (1985), Coronal mass ejections and interplanetary shocks, *J. Geophys. Res.*, *90*(A1), 163–175, doi:10.1029/JA090iA01p00163.

Sheeley, N. R., J. H. Walters, Y.-M. Wang, and R. A. Howard (1999), Continuous tracking of coronal outflows: Two kinds of coronal mass ejections, *J. Geophys. Res.*, *104*, 24,739–24,767, doi:10.1029/1999JA90030.

Sheeley, N. R., et al. (2008), SECCHI observations of the Sun's garden-hose density spiral, *Astrophys. J.*, *674*, L109–L112.

St Cyr, O. C., J. T. Burkepile, A. J. Hundhausen, and A. R. Lecinski (1999), A comparison of ground-based and spacecraft observations of coronal mass ejections from 1980–1989, *J. Geophys. Res.*, *104*, 12,493–12,506, doi:10.1029/1999JA900045.

Stone, E. C., A. M. Frandsen, R. A. Mewaldt, E. R. Christian, D. Margolies, J. F. Ormes, and F. Snow (1998), The Advanced Composition Explorer, *Space Sci. Rev.*, *86*, 1–22, doi:10.1023/A:1005082526237.

Tappin, S. J., and T. A. Howard (2009), Interplanetary coronal mass ejections observed in the heliosphere: 2. Model and data comparison, *Space Sci. Rev.*, *147*, 55, doi:10.1007/s11214-009-9550-5.

Temmer, M., and N. V. Nitta (2015), Interplanetary propagation behavior of the fast coronal mass ejection on 23 July 2012, *Sol. Phys.*, *290*, 919–932, doi:10.1007/s11207-014-0642-3.

Temmer, M., A. M. Veronig, V. Peinhart, and B. Vrsnak (2014), Asymmetry in the CME-CME interaction process for the events from 2011 February 14–15, *Astrophys. J.*, *785*, 85, doi:10.1088/0004-637X/785/2/85.

Thernisien, A., A. Vourildas, and R. A. Howard (2009), Forward modelling of coronal mass ejections using STEREO/SECCHI data, *Sol. Phys.*, *256*, 111–130, doi:10.1007/s11207-009-9346-5.

Thernisien, A. F. R., R. A. Howard, and A. Vourlidas (2006), Modeling of flux rope coronal mass ejections, *Astrophys. J.*, *652*, 763–773.

Thompson, W. T. (2006), Coordinate systems for solar image data, *Astron. Astrophys.*, *449*, 791–803, doi:10.1051/0004-6361:20054262.

Tousey, R. (1973), The solar corona, in *COSPAR Space Research XIII*, pp. 713–730, Akademie, Berlin.

Tucker-Hood, K., et al. (2015), Validation of a priori CME arrival predictions made using real-time heliospheric imager observations, *Space Weather*, *13*, 35–48, doi:10.1002/2014SW001106.

Volpes, L., and V. Bothmer (2015), An application of the stereoscopic self-similar-expansion model to the determination of CME-driven shock parameters, *Sol. Phys.*, *290*, 3005–3022, doi:10.1007/s11207-015-0775-z.

Vourlidas, A., and R. A. Howard (2006), The proper treatment of coronal mass ejection brightness: A new methodology and implications for observations, *Astrophys. J.*, *642*, 1216–1221.

Vourlidas, A., et al. (2015), The wide-field imager for solar probe plus (WISPR), *Space Sci. Rev.*, *204*, 83, doi:10.1007/s11214-014-0114-y.
Vršnak, B., T. Zic, T. V. Falkenberg, C. Mostl, S. Vennerstrom, and D. Vrbanec (2010), The role of aerodynamic drag in propagation of interplanetary coronal mass ejections, *Astron. Astrophys.*, *512*, A43, doi:10.1051/0004-6361/200913482.
Vršnak, B. T., et al. (2013), Propagation of interplanetary coronal mass ejections: The drag-based model, *Sol. Phys.*, *285*, 295–305, doi:10.1007/s11207-012-0035-4.
Wang, Y., B. Wang, C. Shen, F. Shen, and N. Lugaz (2014), Deflected propagation of a coronal mass ejection from the corona to interplanetary space, *J. Geophys. Res. Space Physics*, *119*, 5117–5132, doi:10.1002/2013JA019537.
Wood, B. E., R. A. Howard, and D. G. Socker (2010), Reconstructing the morphology of an evolving coronal mass ejection, *Astrophys. J.*, *715*, 1524–1532, doi:10.1088/0004-637X/715/2/1524.
Yu, H.-S., B. V. Jackson, P. P. Hick, A. Buffington, D. Odstrcil, C.-C. Wu, J. A. Davies, M. M. Bisi, and M. Tokumaru (2015), 3D reconstruction of interplanetary scintillation (IPS) remote-sensing data: Global solar wind boundaries for driving 3D-MHD models, *Sol. Phys.*, *290*, 2519–2538, doi:10.1007/s11207-015-0685-0.
Zhao, X., and M. Dryer (2014), Current status of CME/shock arrival time prediction, *Space Weather*, *12*, 448–469, doi:10.1002/2014SW001060.
Zhao, X., Y. D. Liu, B. Inhester, X. Feng, T. Wiegelmann, and L. Lu (2016), Comparison of CME/shock propagation models with heliospheric imaging and in situ observations, *Astrophys. J.*, *830*, 48, doi:10.3847/0004-637X/830/1/48.
Zheng, Y. (2013), Improving CME forecasting capability: An urgent need, *Space Weather*, *11*, 641–642, doi:10.1002/2013SW001004.